Training toward Advanced 3D Seismic Methods for CO2 Monitoring, Verification, and Accounting

Type of Report: Progress

Frequency of Report: Quarterly

Reporting Period: Oct. 1, 2010 – Dec 31, 2010

DOE Award Number: DE-FE002186 (UH budget G091836)

Submitting Organizations: Department of Earth and Atmospheric Sciences
Allied Geophysical Lab
University of Houston
Houston, Texas 77004-5505

Preparers: Prof. Christopher Liner – P.I.
Phone: (713) 743-9119
Fax: (713) 748-7906
Dr. Jianjun Zeng (research scientist)
Qiong Wu (PHD candidate) … coordinator for this report
Johnny Seales (undergraduate)
Shannon Leblanc (MS candidate)
Bryan Flynn (MS candidate)

Distribution List:

FITS	FITS@netl.doe.gov	DOE-NETL
Karen Kluger	Karen.Kluger@netl.doe.gov	DOE-NETL
Vanessa Stepney	Vstepney@central.uh.edu	UH Contracts Office
Jack Casey	jfcasey@uh.edu	UH EAS Department Chair
Laura Bell	lbell4@uh.edu	UH EAS Department Admin
June Zeng	jzeng2007@gmail.com	Team Member
Qiong Wu	qiongwu2010@gmail.com	Team Member
Johnny Seales	Johnny.seales@gmail.com	Team Member
Lee Bell	lee.bell@geokinetics.com	Geokinetics (Industrial partner)
Keith Matthews	kmatthews@fairfield.com	Fairfield (Industrial partner)
Subhashis Mallick	smallick@uwyo.edu	Univ. of Wyoming
Steve Stribling	SStribling@gmocks.com	Grand Mesa Production

CONTENTS

Executive Summary

This report presents major advances in progress made through the report period from October 1 to December 31 of 2010 for the CO_2 sequestration training project in the Dickman field, Ness County, Kansas (Figure 1).

In this quarter, we continue to study elastic wave model building, lithology zonation interpretation and shear wave estimation. The Gassmann and Xu-White methods are employed as well as empirical methods. In these processes, well log information are input to estimate theoretical shear wave velocity, specifically logs used are sonic (DT), Gamma Ray (GR), density (RHOB) and resistivity (LLD). Results from these three methods show promising consistent features, and are compared to find an optimal shear wave velocity.

We have begun analysis of narrow band spectral decomposition related to fractures and channel features.

Other progress includes work on simulating seismic response to CO2 injection, structural and fault mapping of the Viola formation at the base of the deep saline aquifer, detailed fault/fracture mapping as well as amplitude calibration to well control at the Mississippian unconformity. ?

Lithology Zonation for Humphrey 4-18 Well[1]

The purpose of litho-zonation for Humphrey 4-18 is to estimate lithology as input to the computation of S-wave velocity from the measured P-wave velocity log (sonic DT). We note at the outset that conventional facies identification based on cross-plotting of digital well logs has been unsuccessful at breaking out lithology in the Humphrey 4-18 well (Figure 2).

In the third quarter period, two possible work flows using log discriminators for lithologic zonation were considered and the work load and risks of both methods were evaluated. Since the S-wave calculation at Dickman involves only the Humphrey 4-18 well, in which all required input logs are available from KB to the bottom of the hole, the first and quickest work flow was used in the fourth quarter to establish a litho-zone column.

There are two steps involved in this process. In the first step, a regional geological type-section established at the Schaben 4 well (1 mile away), was correlated to identify major clastics and carbonate litho-sections in Humphrey 4-18 (Figure 3). In the Schaben 4 well, there are no electronic logs from KB to 3500 ft MD depth, only general lithology descriptions available for the correlation at a 20-200 ft scale. Below 3500 ft, direct correlation of gamma ray (GR) and density (RHOB) logs between wells give litho-zone identification. After this general litho-zonation, a detailed litho-zonation was done using Gamma and Photo Electronic logs and the ideal discriminator values (cutoffs) for the end-member lithology (Table 1). For the clastics-dominated sections, GR reading of 80 was used to discriminate the sandstone and shale layers. For the carbonate-dominated sections, the Photo Electronic (PE) reading of 4 was used to further discriminate dolomite from limestone layers. In reality, litho layers in Humphrey 4-18 are mostly mixtures of end-member lithologies, such as sandstone/shale, shale/limestone, and dolomite/chert. These end-member mixtures can have a wide GR range. For example, clean sandstone and chert have GR<40, compared with dirty sandstone with K-feldspar or shale interbeds with GR>80. Limestone or dolomite containing shale inter-beds has GR=40-80, and dolomization of limestone also increases GR>40. The range of PE values for different lithology is mostly overlapped (Table 2). Using single-value cutoffs of end-member lithology may generate errors. Furthermore, the vertical baseline drift of log readings caused by borehole environment may also contribute to the errors.

In the second step, the resulting litho-zones from ideal GR and PE cutoffs were checked against mud logs. The mud log in Humphrey 4-18 well is available only below 3500 ft. Mud logs record rock type as seen in cuttings in the returned drilling fluid with a rather "soft" depth registration based on mud circulation time-lag. Mud log depth resolution cannot match continuous electronic logs to resolve lithology at the logging scale (0.5 and 1 ft), but provides independent validation of the litho-zone results. For example, many

[1] Lead author: June Zeng

mud log sections recorded as limestone and dolomite in carbonate-dominated sections had been classified as sandstone by the ideal GR cutoffs (40-100). Conversely, shale beds seen in mud log (including typical Heebner shale) were classified as dolomite by ideal PE cutoffs. After this detailed correlation, local discriminator values of the end-member lithology were obtain based on statistics (Table 3) and used to refine the litho-zones from the first cycle, especially for the inter-bedded sections of sandstone/shale, shale/limestone, and dolomite/chert . The final litho-zonation is at the scale of 3-20 feet, roughly around the detachability limit of the seismic (11-16 ft) but below the seismic resolution (70-100 ft). This zonation was done in Excel and a typical section near the Mississippian-Pennsylvanian unconformity is shown in Figure 4.

The litho-zone work resulted in the following major lithology sections identified in Figure 2:

Section 1: KB to 1700 ft (surface to Stone Corral) Shale/sandstone dominated sections. Cretaceous bluish-gray shale and marl sequence with thin sandstones as erosional lags.

Section 2: 1700 to 3500 ft (Ninnescah Shale to Kansas City): Interbedded clastics and carbonate rocks, a shallowing-upward sequence with alternating limestone/dolomite, shale, gypsum and evaporate-bearing siltstones/sandstone.

Section 3: 3500 – TD (Marmaton to Osage): Carbonate-dominated sections with shale layers, and some basal sandstone and conglomerates (such as Lower Cherokee Sandstone).

This work also resulted in the following considerations and recommendations for the computation of S-wave velocity using Dr. Han's software.

1. This software is based on the empirical relationship obtained by lab measurements of sandstone and shale, not carbonate samples. It can be used with a certain confidence for the S-wave velocity computation for our section 1 (KB to 1700 ft MD). The following factors should be considered in using the software for the computation of S-wave velocity for our lithology sections 2 and 3.
2. The software requires three input logs in addition to the sonic (P velocity) log. Based on common concepts of the software of this type, these inputs are used to determine the three major factors that may affect the ratio between the vertical and horizontal deformation of the rock body, therefore the P-S wave ratios. The inputs are gamma log for lithology (mineral), density log (probably with resistivity logs) for porosity, and resistivity log for water saturation (fluid types and salinity). The GR log is used basically as a single sandstone/shale discriminator to find the V_{shale} (volume of shale). Therefore in our sections 2 and 3 of the Humphrey 4-18 well, pure carbonate (with low GR) treated as sandstone and carbonate-shale inter-beds (with high GR) as shale, whether the log is standardized or not. The density log (possibly together with resistivity log) gives porosity information for sandstone and shale only. If taking the hard cutoffs, for instance, density 2.5-2.65 as 100% quartz matrix with 0% porosity, it may

consider highly porous carbonates (limestone and dolomite, density 2.7-3.3 as 100% matrix with 0% porosity) in our sections 2 and 3 as tight sandstones. If the density log is standardized, taking the highest density values as tightest rocks, it may underestimate the matrix part and over estimate the porosity of sandstone sections (sections 1 and 2). Given the bad density log in Humphrey 4-18, the results are suspect. Moreover, using only one resistivity log to determine fluid types is also questionable.

3. There is a possible way to minimize the risk of using Han's software. Compared with the fluid types, it seems that the matrix lithology and porosity could have higher weight in generating results. The software also requires the input of bulk modulus, which is much smaller for porous sandstone and shale than for the porous carbonates for 5%-20% porosity. Reports in the literature indicate bulk modulus of SS/SH is approximately 32-18 (10^{10} dynes per square centimeter), while dolomite is 62-34, and limestone 54-23 (Guyod, 1967). If during the Humphrey 4-18 calculation, the input K can vary with litho-zone for our sections 2 and 3 in the computation could be improved and the quality problems of the density and resistivity logs may be partially compensated. For example, one could use $K_{sandshale}$ in section 1, $K_{lime/shale}$ in section 2 and K_{carb} in section 3.

Shear Wave Velocity Estimation[2]

Many efforts have been made to estimate shear velocities in history. With the Gassmann Equation for fluid substitution, we can estimate shear velocities. Greenberg and Castagna (1992) have developed a method based on empirical P-and S-wave velocity relationship in brine sands using measured P-wave velocity to predict shear velocity of sands with different fluid saturation and applying Gassmann Equation to calculate fluid saturation effects, which will be cited as empirical method here. Xu and White (1996) have developed different method that apply Kurster-Toksus porous model to build dry rock with different pore geometry (pore aspect ratio) with constrains of measured porosity and P-wave velocity and fluid saturation effect on velocities estimated by Gassmann equation. Shear modulus and velocity can be estimated based on the dry rock model.

In this section we describe these methods and apply them to the Humphrey 4-18 well to estimate S-wave velocity. However, we are aware that the theory underpinning these methods is based on an assumption of clastic rocks (sandstone and shale), while the Dickman site has significant carbonate in the section. A detailed discussion given above suggests a way the methods discussed here can be used at the Dickman site by treating each of three lithozones separately.

Empirical shear wave velocity estimation

Greenberg and Castagna (1992) developed a general method to predict shear wave velocity in porous, sedimentary rocks which couples empirical relations between shear and compressional wave velocities with Gassmann's equations.

[2] Lead author: Qiong Wu

Xu-White shear wave velocity estimation

Clays are composed of fine sheet-like particles practically, they normally form pores with much smaller aspect ratios than those associated with sand grains. This difference in pore geometry provides the key to obtaining more consistent resistivity and sonic log interpretations. To account for the effect of pore geometry, Xu and White (1995) develop a velocity model for clay-sand mixtures in terms of the Kuster and Toksoz (1974) effective medium and Gassmann theories. In this model, they divide the pore space into compliant shale pores with small aspect ratios and stiff sandstone pores with large aspect ratios. If ϕ denotes porosity, then

$$\phi = \phi_S + \phi_C$$

Where ϕ_S is the portion of the rock occupied by stiff or sandstone pores, and ϕ_C is the porosity associated with compliant or shale pores. The fractional volume of clay comprising the rock matrix, v_C, and sand volume fraction v_S are used to estimate ϕ_C and ϕ_S. Since $v_C + v_S = 1$; assuming that ϕ_C and ϕ_S are proportional to v_C and v_S, respectively, implies that

$$\phi_C = v_C \phi$$

And

$$\phi_S = v_S \phi$$

To estimate compressional and shear-wave velocities of shaley sandstones from porosity and shale content, Xu and White described the elastic properties of the dry frame as

$$K_d - K_m = \frac{1}{3}(K' - K_m)\frac{3K_d + 4\mu_m}{3K_m + 4\mu_m}\sum_{l=S,C}\phi_l T_{iijj}(\alpha_l) \quad \text{------ (1)}$$

And

$$\mu_d - \mu_m = \frac{(\mu' - \mu_m)}{5}\frac{6\mu_d(K_m + 2\mu_m) + \mu_m(9K_m + 8\mu_m)}{5\mu_m(3K_m + 4\mu_m)} \times \sum_{l=S,C}\phi_l F(\alpha_l) \quad \text{----- (2)}$$

Where

$$F(\alpha) = T_{ijij}(\alpha) - \frac{T_{iijj}(\alpha)}{3}$$

In the Kuster-Toksoz equation (1) and (2), K_d, K_m, and K' are the bulk moduli of the dry frame, the rock matrix, and the port inclusion material, respectively, and μ_d, μ_m and μ' are the corresponding shear moduli. For dry rock K' and μ' are zero. Also, α_S and

α_C are the aspect ratios for the stiff and compliant pores; $T_{iijj}(\alpha)$ and $F(\alpha)$ are pore aspect ratio functions derived from the tensor T_{ijkl} that relates the uniform strain field at infinity to the strain field within an elastic ellipsoidal inclusion (Wu, 1966).

Given the dry rock elastic moduli, Xu and White (1995) use Gassmann's equations (White, 1983, p 60) to calculate the fluid saturated bulk and shear modulus, from which compressional and shear-wave velocity can be found

$$K = K_d + \frac{\left(1 - \frac{K_d}{K_0}\right)^2}{\frac{\phi}{K_f} + \frac{(1-\phi)}{K_0} - \frac{K_d}{K_0^2}},$$

$$\mu = \mu_d,$$

$$\rho = \phi\rho_f + (1-\phi)\rho_0,$$

$$V_P = \sqrt{\frac{\left(K + \frac{4}{3}\mu\right)}{\rho}},$$

And

$$V_S = \sqrt{\frac{\mu}{\rho}}.$$

In above five equations, *K is* the bulk modulus of the fluid saturated rock, K_f is the bulk modulus of the pore fluid, and μ denotes the shear modulus of the fluid-saturated rock. Also, ρ_0 is the density of the rock matrix, ρ_f is the fluid density, and ρ is the density of the fluid saturated rock. Finally, V_P and V_S are the compressional- and shear-wave velocities of the fluid-saturated rock.

With this procedure, Xu and White (1995) were able to accurately predict compressional- and shear-wave velocities of shaley sands.

Gassmann's shear wave velocity estimation

Velocity at in-situ saturation conditions can be calculated from the dry-rock velocity using fluid substitution equations (Gassmann, 1951), which based on dry hexagonal packing of spheres theoretical relation and shows below.

$$V = 800 \left[\frac{2\pi E^2 g}{(1-\sigma)^2 \phi^3 \rho} \right]^{1/6} z^{1/6}$$

E =Young's modules of spheres
σ =Poisson's ratio of spheres
ρ = density of spheres
ϕ = porosity of medium

A newly method, which uses the optimal method for estimating the properties of dry rock and Gassmann equation to predict the S wave velocity, is proposed by Dr. Dehua Han. And this is one of the three methods we utilized to estimated S wave velocity.

Shear wave velocity results

With courtesy of Dr. Dehua Han, software incorporating the three methods given above was used to estimate shear velocity in the Humphrey 4-18 well at the Dickman site. This well has sonic, gamma ray, resistivity and density logs from 186 ft to 4593.5 ft with a 0.5 ft interval (see in Figure 5).

The Humphrey 4-18 is chosen since it has more complete log coverage than our other deep candidate well (Sidebottom 6, see Figure 6) for the estimation process.

However, the log quality of Humphery 4-18 is not ideal, a fact that could limit the S wave estimation quality. Density log values shows a zigzag distribution, local high density values alternate with anomalously low density values throughout the well, including the shallow section from 56-1060 m. Resistivity has a relatively consistent trend with values below 100 ohm-m, but there are a number of anomalously high resistivity intervals with values as high as 100000 ohm-m distributed randomly throughout. These anomalies could corrupt the Vs estimation accuracy.

Clay content is estimated from gamma ray, water saturation from resistivity, and porosity from density. It can be seen that the predicted S wave velocity profiles are very similar (Figure 7) both in general trend and in location of extreme values. The empirical method gives a relatively low estimation, which may indicate that local calibration is be necessary.

The estimated S wave velocity from each method is plotted with the observed P wave velocity from sonic log in Figure 8.

Vs Estimation Summary

We have now investigated several methods of estimating shear wave speed at well log resolution. A global VsVp ratio is too simple to capture the lithologic variability at Dickman. While Han's approach is elegant, it suffers from a lack of carbonate rock physics and it relies completely on well log data that is known to be unreliable in the Humphrey 4-18 well.

The method that combines geological knowledge, all available logs, and mud log information gives our best estimate of lithology. Combining this with typical VsVp ratios in each lithology will generate a shear wave sonic log from the existing P-wave sonic with only slight discontinuity at the lithologic boundaries. We intend to build the shear sonic in this way for use in ANIVEC for elastic data simulation in the next quarter.

Spectral Decomposition

In our ongoing effort to investigate seismic attributes to geologic features at Dickman, we have generated a series of narrow-band attribute volumes from the migrated data. Unlike traditional time-frequency methods (Chakraborty and Okaya, 1994) that seek a trade-off of time and frequency resolution, we have chosen to use a pure frequency isolation algorithm. In fact, the method we use is traditional Fourier bandpass filtering with a very narrow response centered on the frequency of interest. In Figure 9 we show (a) the original 3D migrated data spectrum as extracted in a 5x5 bin area, (b) the same after narrow band filtering around 6 Hz and (c) after 43 Hz narrow band filtering.

In the vertical view (Figure 10) the narrow band results are not very enlightening. It is tempting to conclude the new data has no time information content, but in fact there is time localization in the amplitude of each trace although it seems to have little value in the vertical view.

Figure 11 shows a time slice through the broadband data at 848 ms, roughly coincident with the Miss/Penn unconformity. The prominent incised channel is clearly shown. Note there are no clear trends in the data aligned with the yellow dash lines and the channel does not seem to approach the tip of the yellow arrow.

A coincident time slice through the 6 Hz data (Figure 12) shows a strong and remarkable diagonal alignment parallel to the yellow dash lines. We suspect these features indicate fracture orientation as described using curvature by Nissen et al. (2004, 2006). We plan to investigate this alignment further in the next quarter.

At a higher frequency band (43 H, Figure 13) we observe a dark channel-like feature as indicated at the tip of the yellow arrow. We are currently working to confirm or deny the reality of this channel feature. The process will consist of studying well logs inside and outside the feature; particularly concentrating on basal Pennsylvanian sediments and indications of a subtle structural low at the top Mississippian.

Channels exhibit traits, such as facies successions, that permit identification. It is important to not only examine the logs that lie within the expected channel, but also those outside it. The characteristics of these two locations should be different. There are two main types of channels that could be represented here. Specifically, the possibility of a braided or meandering river. There are different characteristics that classify both, but there are similarities. The overall facies successions within these units are characterized as fining upward sequences. This takes into account the coarser sands that are cross bedded that fine into the silty or muddy deposits. In a core section this would be

recognizable as a fluvial system. Bioturbation of nonmarine creatures and plant roots might also be present in the finer grains. Orgranics may also be present at the flooding surfaces from when the channel increased in velocity, jumped its banks, and began to flow in a more linear fashion. These types of successions are more likely to be found outside the levees of the river.

Previously listed characteristics can be taken into account while interpreting the log responses of the surrounding wells. The rock properties measured by the gamma log may reproduce the fining upward signature of a channel. The reasoning behind this is sand and more muddy lithologies will have different responses. This fining upward sequence will also exhibit the flooding surfaces that cause this process in the flood plains allowing for correlation and interpretation of the paleoenvironment.

Seismic Response to CO_2 Injection[3]

Seismic simulation

The current CO2 flow simulation calculations utilize the Computer Modeling Group (CMG) generalized equation of state compositional simulator (GEM) which can be used in CO2 enhanced oil recovery and CO2 storage. The flow simulation outputs include reservoir properties for each grid cell, including depth, porosity, pressure and fluid saturation. We are importing these properties into software implementing the Gassmann equation to calculate fluid saturated rock velocity and density in each simulation grid cell as a function of time. The velocity and density combine to give acoustic impedance. Time-lapse seismic response is directly related to the impedance contrast between two adjacent layers, and thus a new seismic volume can be generated to analyze the reservoir reflectivity at different simulation times. In this work, our first approach uses a simple convolutional model in which computed normal-incidence reflection coefficients are convolved with a seismic wavelet (Ricker). We anticipate a more sophisticated finite difference full wave forward modeling engine will be investigated in the future.

Data Preparation

The CMG flow simulation output is a set of reservoir property grids that we import to Matlab as 3D volumes of dimension (nx,ny,nz)=(33,31,32). The simulation grid upper surface is at +150 ft subsea depth (seismic datum is at +2600 ft). The grid cells have uniform lateral dimension (dx,dy)=(500,500) feet and origin in the southwest corner at absolute coordinates (1562247, 690023) feet coincident with the Dickman field 3D seismic data origin. The simulation grid depth increment (dz) is variable to represent thickness of geological layering and loss of section due to an unconformity at about -1980 ft subsea.

In the current testing phase we simulate seismic response in each 500x500 ft simulation grid cell. Moving forward, however, we will interpolate this very coarse simulation grid

[3] Lead author: Jintan Li

to the finer seismic bin grid of 82.5x82.5 ft to facilitate comparison of field seismic data to flow grid seismic simulation results. We hope to use the field seismic data to validate the initial (pre CO2 injection) flow simulation case.

An impedance volume can be generated using simulation grid property inputs and the Gassmann theory of velocity and density calculation for porous fluid saturated rock. Here I show an example at the early stage of injection, when pores are brine-filled, and after 50 years. Even at the later time very little CO2 resides in the storage target (Osage deep saline aquifer), and thus the impedance results largely depend on porosity distribution. Figures 14 and 15 show the time-zero computed impedance distribution for 32 layers. The impedance is constant in layers 2-4 because the simulator grid has constant porosity for those layers.

Stripes seen in some impedance slices may be caused by poor interpolation of sparse porosity values from well logs. These interpolation artifacts did not much affect the flow simulation results as evidenced by a good history match. But they will have a strong influence on seismic response, representing a challenge for simulating seismic data from flow grids.

Notice that there are some missing areas (white) shown on the impedance slices associated with the Mississippian-Pennsylvanian unconformity, where a shallow target of the CO2 storage is located. Figure 16 gives detailed impedance variation (on a different color scale) for layers spanning the unconformity, again missing section is white.

Reflection coefficients calculation

Ro is calculated by the impedance contrast between two adjacent layers:

$$R_0 = \frac{I_n - I_{n-1}}{I_n - I_{n-1}} \ldots\ldots \qquad n=2,3,\ldots,32$$

I_n : Impedance for the n^{th} layer

There are 32 depth layers in each (x,y) simulation cell, represented by one depth column with 32 points. Due to the unconformity some depth points are missing. This situation is handled by the following procedure:

1. If a data point is missing for a particular layer, the reflection coefficient is set to zero. Ro for the layer above is calculated from the impedance of the layers above and below the missing layer.
2. If multiple data points are missing for a fixed (x,y) location, the reflection coefficients are assigned zero for all these layers. Ro for the non-zero layers are attained by the difference between those two nearest layers where impedance values are nonzero.

After reflection coefficients have been calculated for all layers, a depth-to-time conversion needs to be performed. This is required for time-domain convolution with the Ricker wavelet. A time-depth function generated from the Dickman 6 well sonic curve is used to obtain reflectivity at each calculated time (1 ms time sample rate). Since the time

samples are quite sparse and not evenly distributed, a polynomial interpolation is applied to generate regularly time-sampled data. A 35Hz Ricker wavelet was used to convolve with the calculated reflectivity and generate the seismograms as shown in Figures 17a and 17b. These seismograms indicate the data as it would appear before CO2 injection, time zero of the simulation run.

The simulation seismic dataset consists of 33 inline traces and 31 crossline traces. Notice lateral inconsistency in the seismic, mainly due to the large distance between adjacent traces. This should be reduced when (x,y) interpolation is done from the simulation grid scale (500 ft) to the seismic bin scale (82.5 ft). Application of a smoothing operator may also help to resolve this issue.

However, this preliminary result still provides some useful information. The first strong reflection shown on seismic corresponds to the starting depth of the flow simulation grid, and stronger reflections show details of layer thickness, porosity, and pore fluid variation represent the unconformity locations. Future work will incorporate a better-defined interpolation algorithm and a more accurate depth to time conversion into the simulation process to obtain more realistic seismic data. In this way, the comparison between different seismic attribute analyses due to changes of rock and fluid properties at various times will be effectively carried out in the later investigations.

Deep Structure Mapping[4]

Last quarter we concluded that only two out of the four deep wells were viable for synthetic seismogram generation, specifically Sidebottom 6 and Humphrey 4-18. Synthetic seismograms were created for these wells, but there were a few problems (Figure 18):

1) The Humphrey 4-18 is on the edge of the 3D seismic area
2) The Sidebottom 6 is outside the 3D seismic area
3) Both synthetics had a correlation coefficient well below 0.1
4) Humphrey 4-18 has questionable logs

To address these problems, we 'moved' the Humphrey 4-18 and Sidebottom 6 into the 3D seismic area by creating dummy wells DH-4-18 and DS6, see Figure 19. This is justified since most horizons are laterally continuous (layer cake geology, see Figure 3). These dummy wells were placed inside the survey area, away from edge effects, but as near as possible their original locations. They also contained all the same well parameters as their original well, except the DS6 used tops from the Stiawalt 3 since it is slightly closer than the original Sidebottom 6 well.

Parameters of the synthetic wavelets from both DH-4-18 and DS- 6 include an extraction of the wavelet using a 500 ft. radius at the borehole, sample interval of 2 milliseconds, wavelet length of 0.1 seconds, and time interval 0.75–1.25 s.

[4] Lead author: Shannon LeBlanc

The DH-4-18 synthetic used both a clipped density and a clipped sonic log. The synthetic wavelet extracted was from 116 traces and the synthetic correlation coefficient was R=0.115. This R-value was before any phase shift was attempted. The phase shift (PS) that produced the best visual match was -180 degrees. Unfortunately the R-value dropped even lower leaving a value of R = 0.112, see Figure 20.

DS-6 used the original sonic log and a clipped density log. The wavelet was extracted from 112 traces and had the synthetic had a correlation coefficient of R = 0.362 before with no PS. A PS of 53 degrees showed the best visual match and gave a much better value of R = 0.603, see Figure 21.

After a comparison between the DH 4-18 and the DH-6 synthetic seismograms (see Figure 22), a decision was made to move forward using only the DS-6 well to tie the geology to the seismic.

Looking at the phase shifted synthetic in a vertical section in Figure 19, it was noted that the Osage lies at the base of a trough (near zero crossing), Gilmore City lies at the base of a peak, and Viola lies at a zero crossing. Therefore, the Osage will be picked at a trough and attributes extracted a few ms above the horizon. The Gilmore City will be picked at a peak and Viola at a zero crossing. Offset tracking will be used to extract attributes by time-shift away from these tracked events.

Summary of Significant Events

The primary purpose of this research is to simulate a 3D 3C seismic survey over the Dickman area. Estimation of the shear wave velocity profile is key to this effort, and we have settled on a final method of approach this quarter.

Work Plan for the Next Quarter

By next quarter we will utilize forward modeling to test the effect of density, to see if we could avoid using the Humphrey 4-18 density log that is in poor quality. We will continue working on estimating optimal S wave velocity.

We will continue working on flow simulator to seismic simulation methods. A better defined interpolation algorithm and a more accurate depth to time conversion will be incorporated into the simulation process to obtain seismic datasets with better resolution. Comparisons of seismic images at period times will be carried on as research progresses.

We will continue refining synthetics and further interpretation on Viola, interpret time and depth structure maps towards this formation, run multiple attributes, and eventually estimate storage capacity and depth conversion.

Future work on spectral decomposition will be to validate the 43 Hz channel feature with well log control at the unconformity.

Cost and Milestone Status

Baseline Costs Compared to Actual Incurred Costs….

8/1/10 – 12/31/10	Plan	Costs	Difference
Federal	$36,668	$25,188	$11,480
Non-Federal	$4,063	$0	$4,063
Total	$40,730	$25,188	$15,552

Forecasted cash needs vs. actual incurred costs

Notes:
(1) Federal plan amount based on award of $293,342 averaged over 8 reporting quarters.
(2) Non-Federal plan amount based on cost share of $32,500 averaged as above.
(3) Cost this period reflects salary for J. Zeng (3 mo), Q. Wu (3 mo), and J. Seales (3 mo).

Actual Progress Compared to Milestones

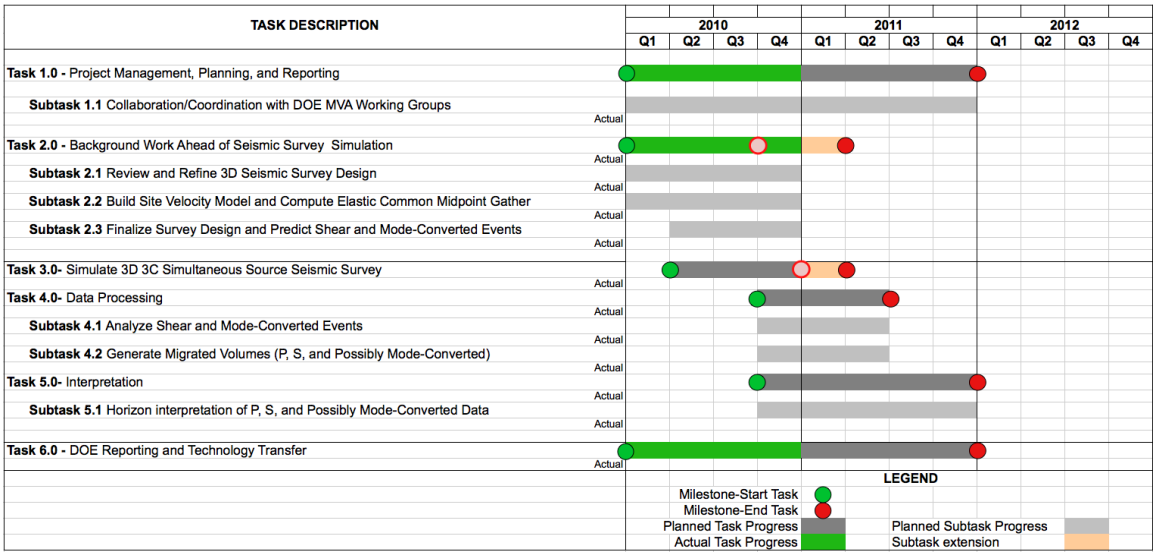

Continuing Personnel

Prof. Christopher Liner is Principle Investigator and lead geophysicist. He is a member of the SEG CO_2 Committee, Associate Director of the Allied Geophysical Lab, and has been selected to deliver the 2012 SEG Distinguished Instructor Short Course.

Dr. Jianjun (June) Zeng has been working exclusively on this project since Dec 2007 and is lead geologist.

Ms. Qiong Wu is a graduate PHD student in geophysics who joined the project in January 2010 as a research assistant. She will be funded year-round out of the project.

Mr. Johnny Seales is an undergraduate student majoring in Geology and Geophysics. He is also a U.S. Army veteran, having served in Iraq. He will be funded year-round from the project. He anticipates earning his undergraduate degree in Dec. 2011.

Ms. Jintan Li is a 2nd year PhD student in geophysics who joined the project in Aug 2009. She is funded by Allied Geophysical lab at this time. Her thesis will be time-lapse seismic modeling (4D) for conducting dynamic reservoir characterization of the Dickman Field.

Ms. Shannon Leblanc received her bachelor's in geology at the University of Louisiana at Lafayette and is now pursuing a master's degree in geophysics at the University of Houston. She is the current SEG student chapter president and joined the CO2 group in January of 2010. Shannon is mapping deep structure in the Dickman Field to determine the potential of a deep saline aquifer as a co2 storage candidate.

Mr. Eric Swanson is a part time graduate MS student in geophysics who joined the project in July 2010.

Technology Transfer Activities

Two presentations are accepted for presentation at the AAPG and SPE Annual Meeting. They are:

3D Geologic Modeling toward a Site-specific CO2 Injection Simulation by Jianjun Zeng,

A CO_2 Sequestration Simulation Case Study at the Dickman Field, Ness Co., Kansas by Christopher L. Liner, see appendix 1 and 2 for detail.

Contributors

Christopher Liner (P.I, Geophysics)
Jianjun (June) Zeng (Geology and Petrel Modeling)
Qiong Wu (Geophysics PhD candidate)
Johnny Seales (Geology and Geophysics Undergraduate)
Jintan Li (Geophysics PhD candidate)
Shannon Leblanc (Geophysics MS candidate)
Bryan Flynn (Geophysics MS candidate)
Eric Swanson (Geophysics MS candidate)

References

Chakraborty, A. and Okaya, D., 1995, Frequency-time decomposition of seismic data using wavelet-based methods: Geophysics, Soc. of Expl. Geophys., 60, 1906-1916.

Han D. H., and Batzle M. L., 2002. Simplified and constrained Gassmann's equation. Presented at SEG annual meeting Salt Lake City.

Dehua Han, Michael Batzle, Estimate Shear Velocity Based on Dry P-wave and Shear Modulus Relationship,

Fritz Gassmann, 1951, elastic eaves through a packing of spheres,

Greenberg, M. L., and Castagna J. P., 1992. Shear-wave velocity estimation in porous rocks: Theoritical formulation, preliminary verification and application.

Kuster, G. T., and Toksoz, M. N., 1974, Velocity and attenuation of seismic waves in two-phase media: Part 1: Theoretical formulation: Geophysics, Vol. 39, 587–606.

Nissen, S. E.,T. R. Carr, and K. J. Marfurt, 2006, Using New 3-D Seismic attributes to identify subtle fracture trends in Mid-Continent Mississippian carbonate reservoirs: Dickman Field, Kansas, Search and Discovery, Article #40189.

Nissen, S. E., K. J. Marfurt, and T. R. Carr, 2004, Identifying Subtle Fracture Trends in the Mississippian Saline Aquifer Unit Using New 3-D Seismic Attributes: Kansas Geological Survey, Open-file Report 2004-56.

Robert G. Keys and Shiyu Xu. 2002, an approximation for the Xu-White velocity model, Geophysics, Vol. 67, NO. 5 (Sept.-Oct. 2002); P. 1406–1414.

WELLOG web page: Guyod, Geophysical Well Logging, 1967, http://www.wellog.com

Xu, S., and White, R. E., 1995, A new velocity model for clay-sand mixtures: Geophysics Prospecting, 43, 91–118.

Xu, S., and White, R. E., 1996, A physical model for shear-wave velocity prediction: Geophysical Prospecting, 44, 687-717.

Appendix I

3D Geologic Modeling toward a Site-specific CO2 Injection Simulation.
Jianjun Zeng[1], Christopher L. Liner[1], Po Geng[1], Heather King[1],

A solid geological model at reservoir scale is the key starting point toward a site-specific characterization of a CO2 sequestration target. In the Dickman Field of Ness County, Kansas, a 3D structure and property model was built for depleted reservoirs of carbonates and clastic rocks through multi-scale data integration. Work flows were designed to handle some of the challenges commonly involved in geological modeling at the reservoir-scale: targeting geological features normally considered as "sub-seismic" and beyond the resolution of conventional seismic stratigraphy; recognizing the lateral heterogeneity in acoustic properties of laterally interwoven clastics and carbonate lithologies on a karst-modified paleo-topography to restore true subsurface geometry; calibrating legacy well logs to obtain reservoir properties with quantified risk assessments; and extracting a fault-fracture framework from multiple seismic attribute volumes to guide the reservoir property gridding.

As a first step, a depth-converted stratgraphic model was established and validated by log interpretations at 17 well sites. Fault and fracture analysis was based on seismic interpretation and volumetric attributes, supported by log and core evidences and understanding of the regional deformation history. A unique set of porosity was assigned to the stratigraphic model through calibrating porosity logs of different types and correlating log to core measurements. Permeability estimation was based on core measurements available in Dickman and the surrounding oil fields. Water saturation measured from flushed cores was calibrated to the in-situ water saturation. The propagation of these reservoir properties through the model was along preferred orientations guided by fracture and acoustic impedance analysis. The resulting property grid was tested by production history-matching simulation. A reasonable match was obtained after two rounds of input parameter adjustment and the inclusion of a capillary zone in the model.

The initial geological model built from heavily drilled reservoirs was extended to deeper saline aquifers with only three well controls, aided by 3D seismic impedance analysis. The grid served as input to CO2 injection simulations for the deep saline aquifer, a potential carbon capture and sequestration target.

Appendix II

A CO_2 Sequestration Simulation Case Study at the Dickman Field, Ness Co., Kansas
Christopher L. Liner, Po Geng, Jianjun Zeng, Heather King and Jintan Li, U. of Houston

Since 2006 The University of Houston has evaluated CO_2 sequestration potential in a deep saline aquifer system in Ness County, Kansas. This paper is a summary on the simulation part of the project.

Combining 3D seismic and dense well control, a static model was constructed and history matching was accomplished. Lack of pressure data and early records of water production complicated history matching validation. An acceptable result was obtained only after many iterations and model modifications.

After history matching, various aquifer simulation models were constructed to study the CO_2 injection rate and storage safety issues. A full formation simulation model including sallow geological layers and deep saline aquifer was further constructed to predict CO_2 migration after injection.

Free CO_2 gas trapped in a geological structure can migrate to the surface through faults, fractures, failed cap rock, or corroded well pipe. These actions represent a real safety threat. A major challenge is to develop a practical simulation model to study CO_2 leakage scenarios over long time periods (typically 250 years in our work). One way of improving CO_2 storage safety is to accelerate residual gas and solubility trapping. Our simulation results indicate two effective ways of reducing free CO_2: injecting CO_2 with brine, and/or horizontal well injection. In the carbonate aquifer we studied, tuned combination of these methods can reduce the amount of free CO_2 from over 50% to less than 10%.

As part of the lower Paleozoic aquifer systems in Kansas, Missouri and Oklahoma, the site under the Dickman oil field shows the potential as an viable CO_2 storage site. However, faulting and numerous abandoned wells cast uncertainty on its ability to serve as a permanent CO_2 storage site. This study shows that a careful simulation study can maximize CO_2 injection rate, minimize existence of free CO_2, and significantly reduce uncertainty in the safety of CO_2 permanent storage.

Tables

Minerals (rocks)	PE	GR
Calcite	5.084	0-5
Dolomite	3.14	5-20
Shale	3.42	>80
Dirty Sandstone	2.70	>30
Clean Sandstone	1.75	1-30

Table 1. Theoretical log values for the end-member minerals

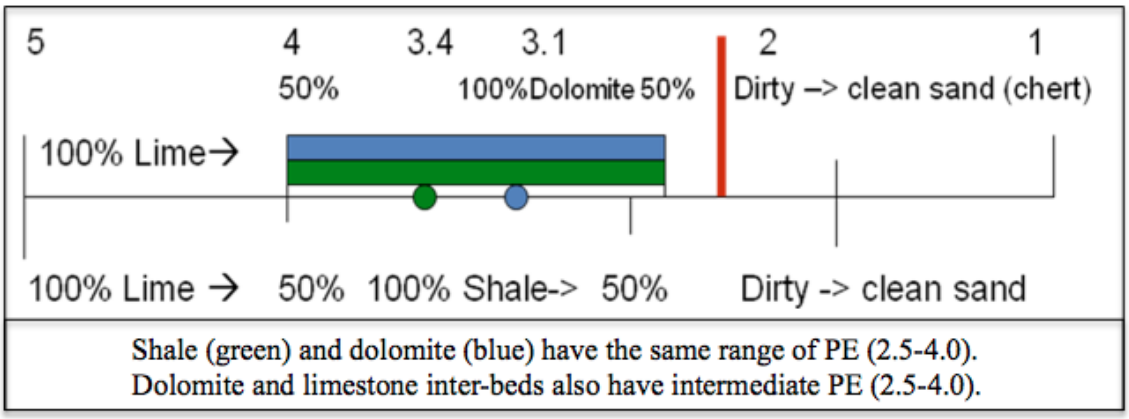

Table 2. PE log value ranges for different lithology.

Lithology	Average PE	Average GR
limes	4.3	34
Lancing Group Limestone	4.1	26
Heebner Shale	5.1	230 (carbonaceous)
Cherokee Group shale	3.8	182
Cherokee Group Sandstone	3.4	56
Cherty sandstone and conglomerates	2.9	38
Dolomite	3.0	34

Table 3. Statistics for different lithologies in Humphrey 4-18 well.

Figures

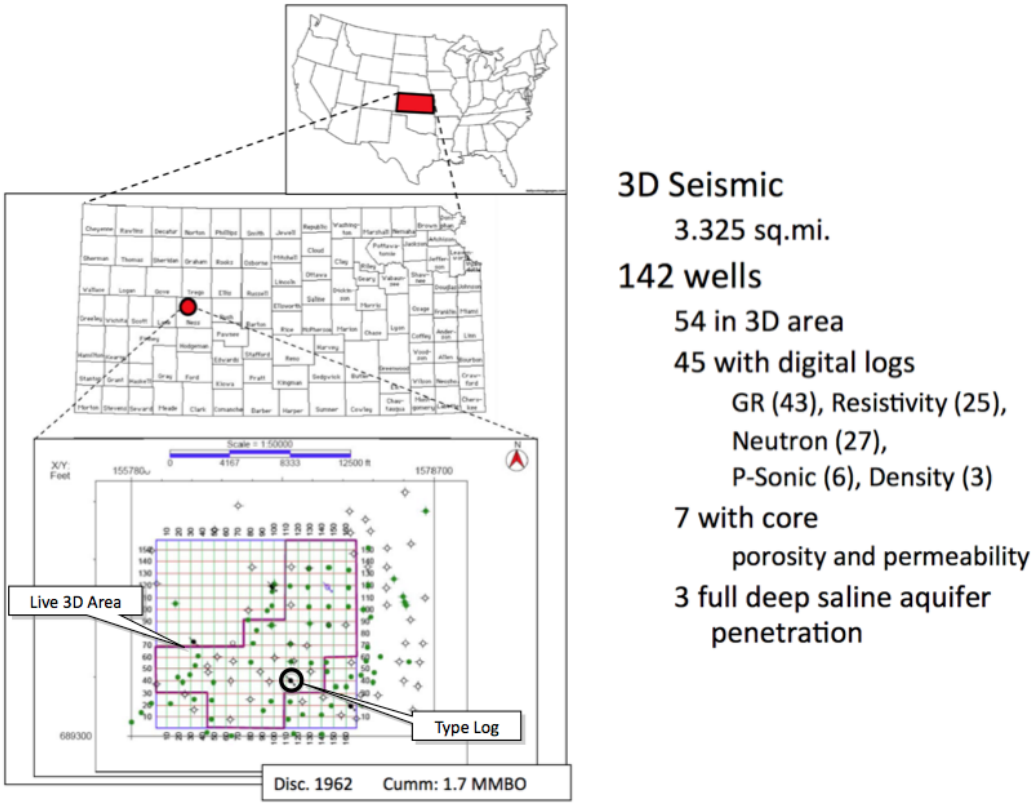

Figure 1. Dickman field site and description of available data.

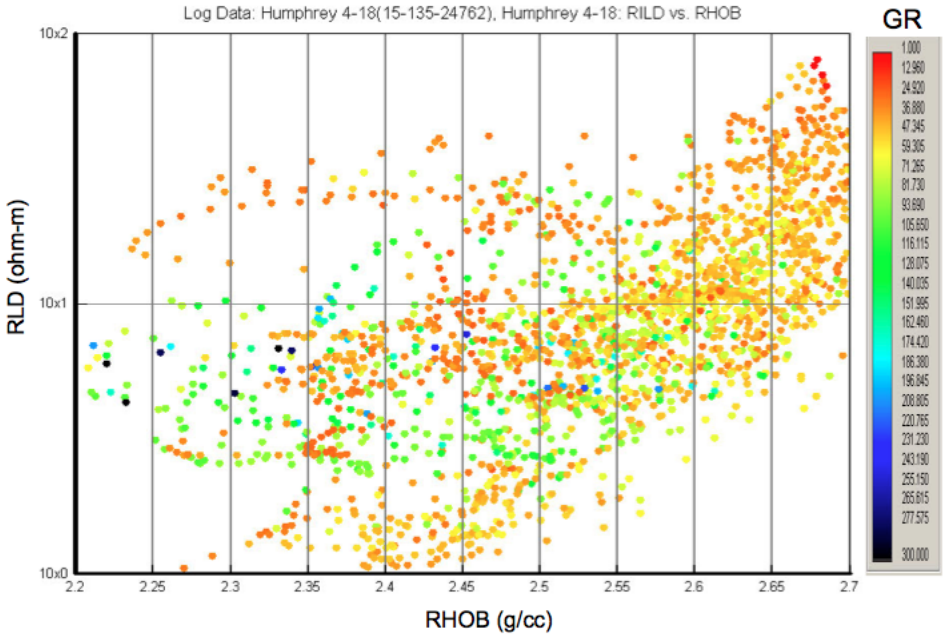

Figure 2: Conventional Humphrey 4-18 facies plot from 3500 to 4450 ft measured depth. The cross plot is density and deep resistivity colored by gamma ray log values (see colorbar). Note the lack of specific breakouts into lithological groups.

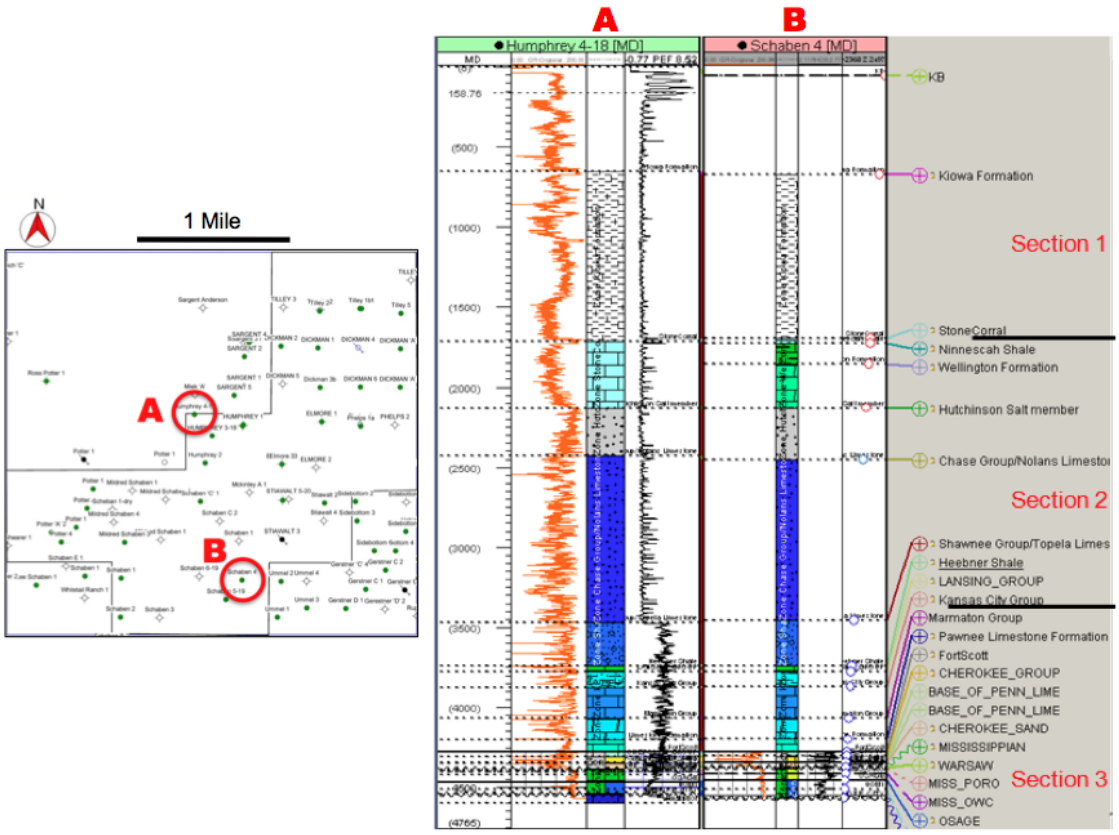

Figure 3. Stratigraphic Correlation of Humphrey 4-18 (green) well to the type-section in Schaben 4 (pink) well. Well locations are shown in the reference map to the upper right.

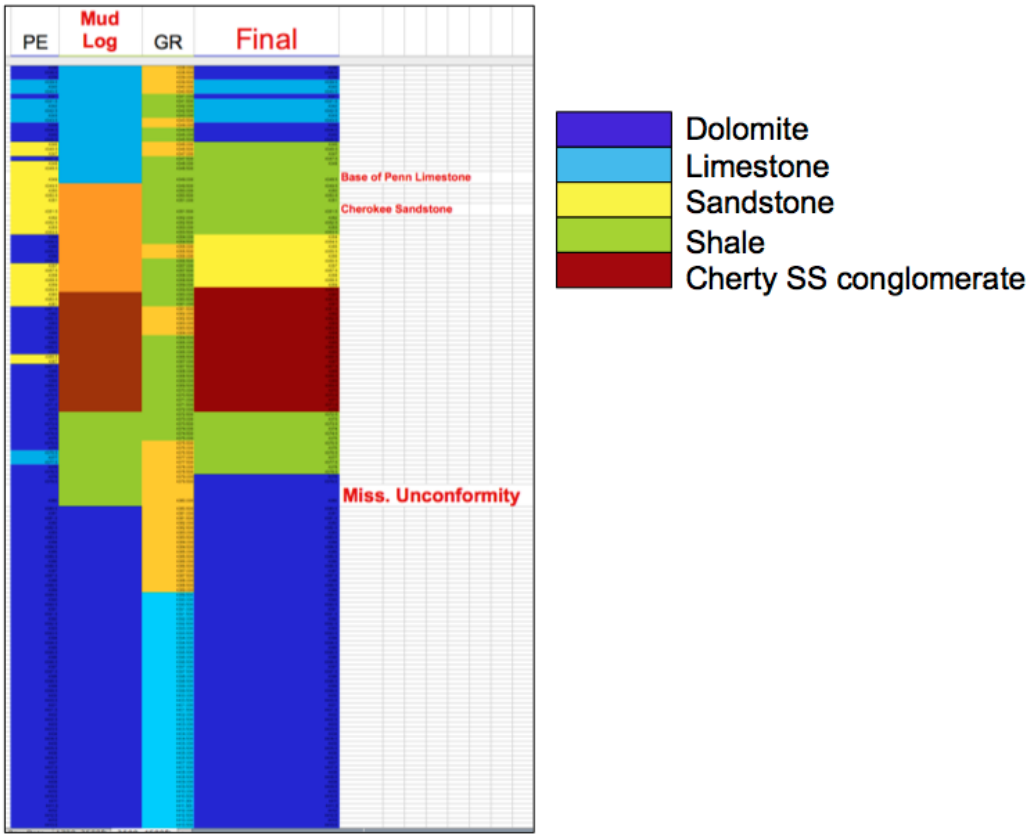

Figure 4. Final Humphrey 4-18 lithozones across the Mississippian-Pennsylvanian boundary based on fundamental geological analysis.

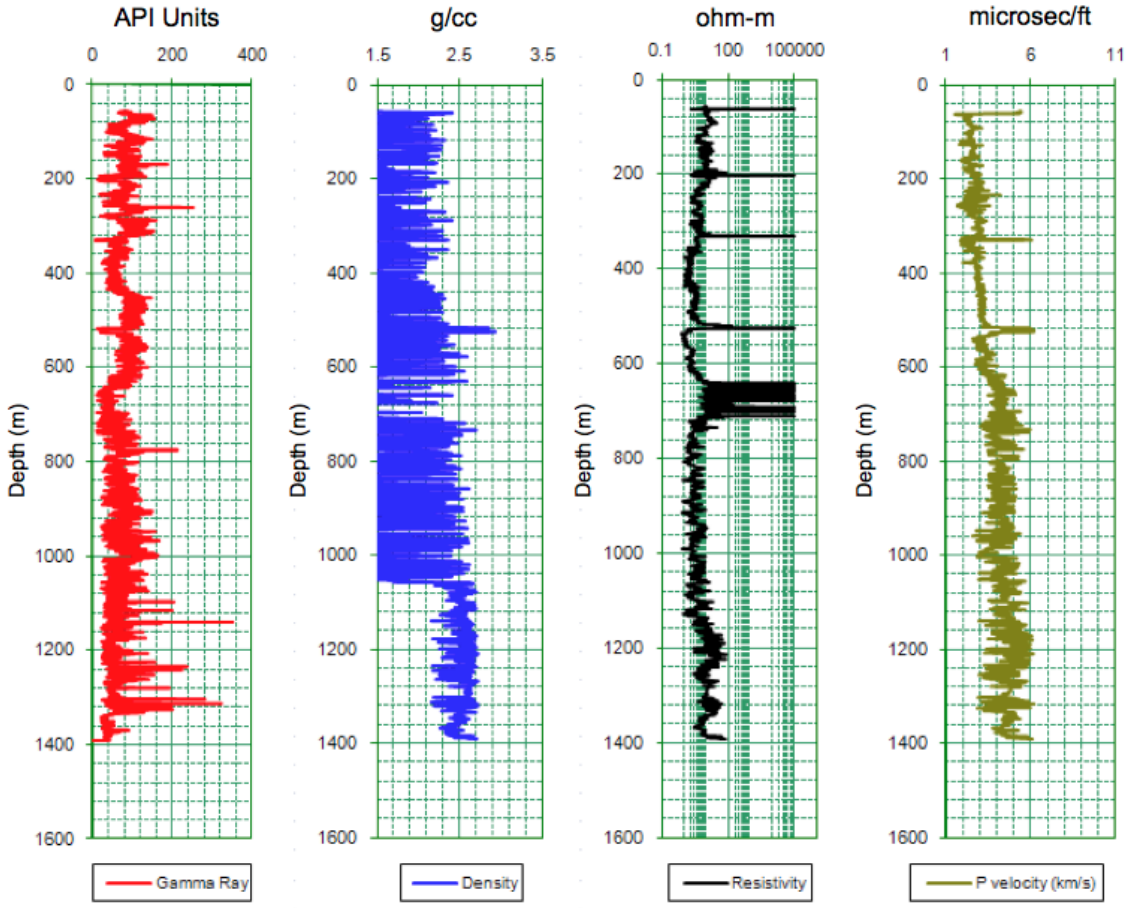

Figure 5. Humphery 4-18 well logs input to Dr. Han's shear velocity estimation process.

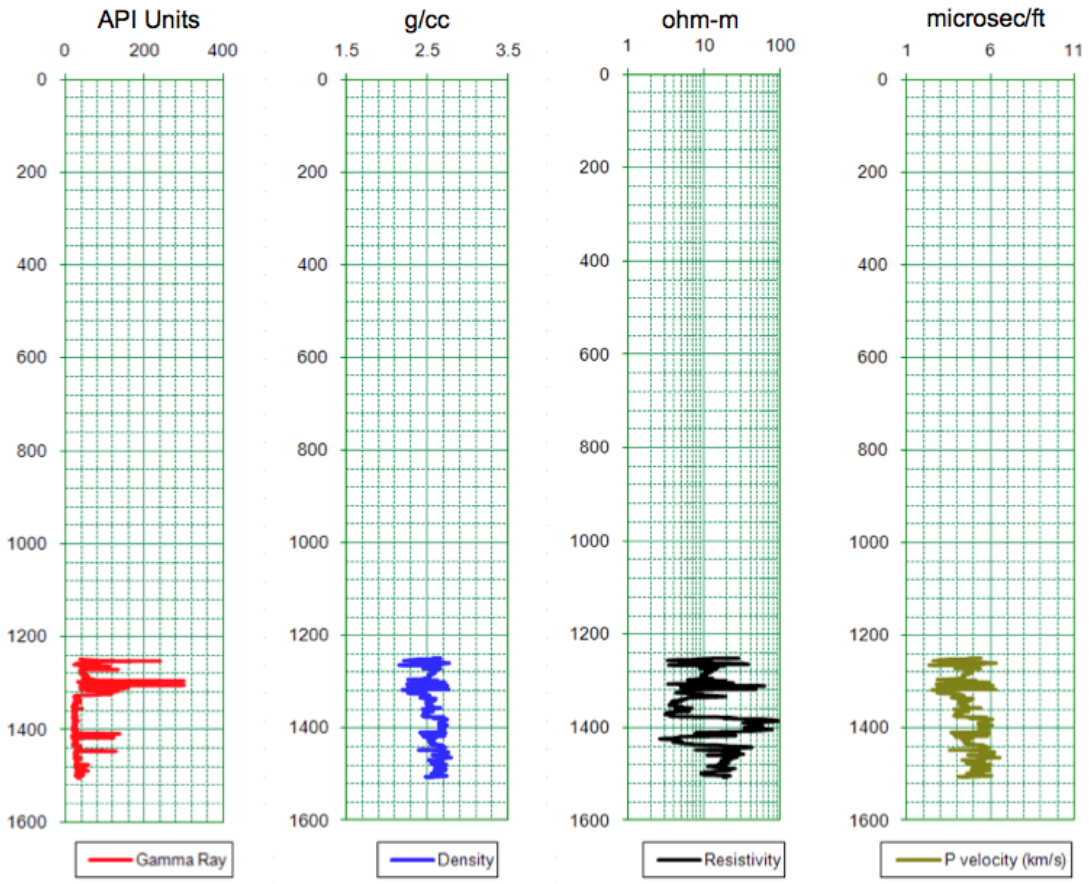

Figure 6. Sidebottom 6 well log coverage rules out this deep well for shear velocity estimation.

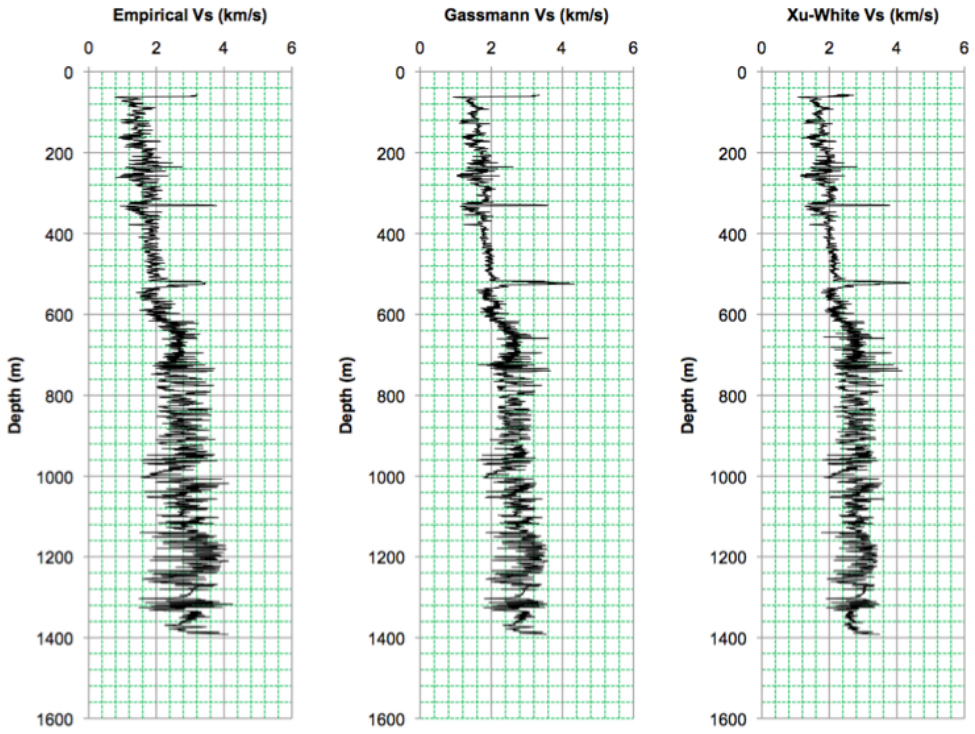

Figure 7. Humphery 4-18 Vs estimation from Empirical method, Gassmann method and Xu-White method.

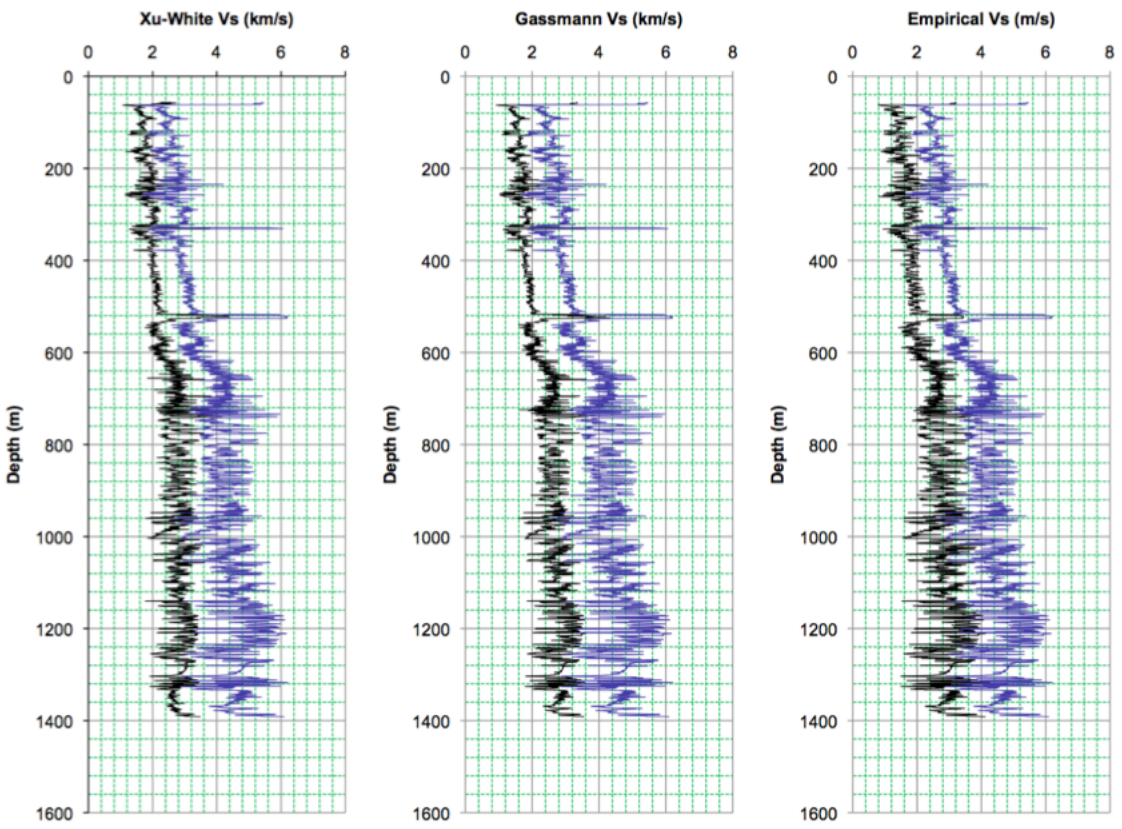

Figure 8. Humphery 4-18 Vs and Vp plots for Vs estimated from Empirical method, Gassmann method and Xu-White method respectively.

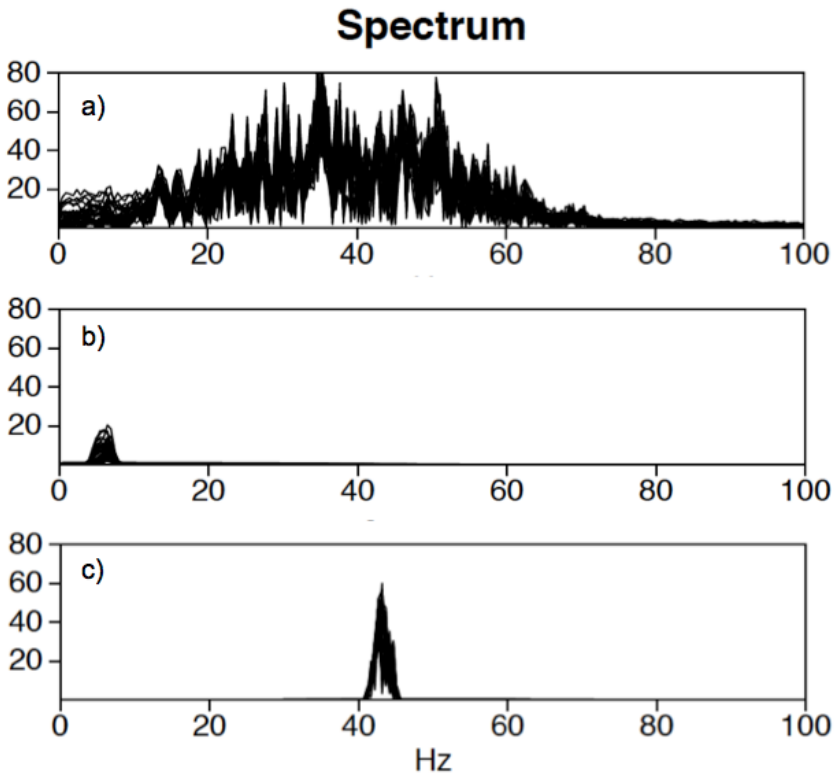

Figure 9. Spectrum of Dickman seismic data and narrow band decomposition. (a) Fourier amplitude spectrum of 3D migrated data in a 5x5 bin area from 0-2 seconds. (b) Spectrum after narrow bandpass filtering centered on 6 Hz. (c) Spectrum after 43 Hz narrow bandpass filtering.

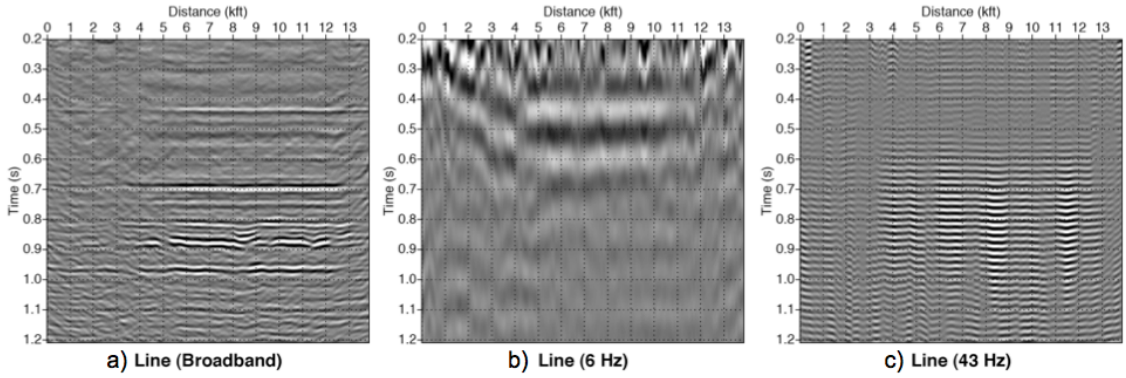

Figure 10. Representative seismic line before and after filtering. (a) Original broadband data. (b) Narrow band 6 Hz data. (c) Narrow band 43 Hz data.

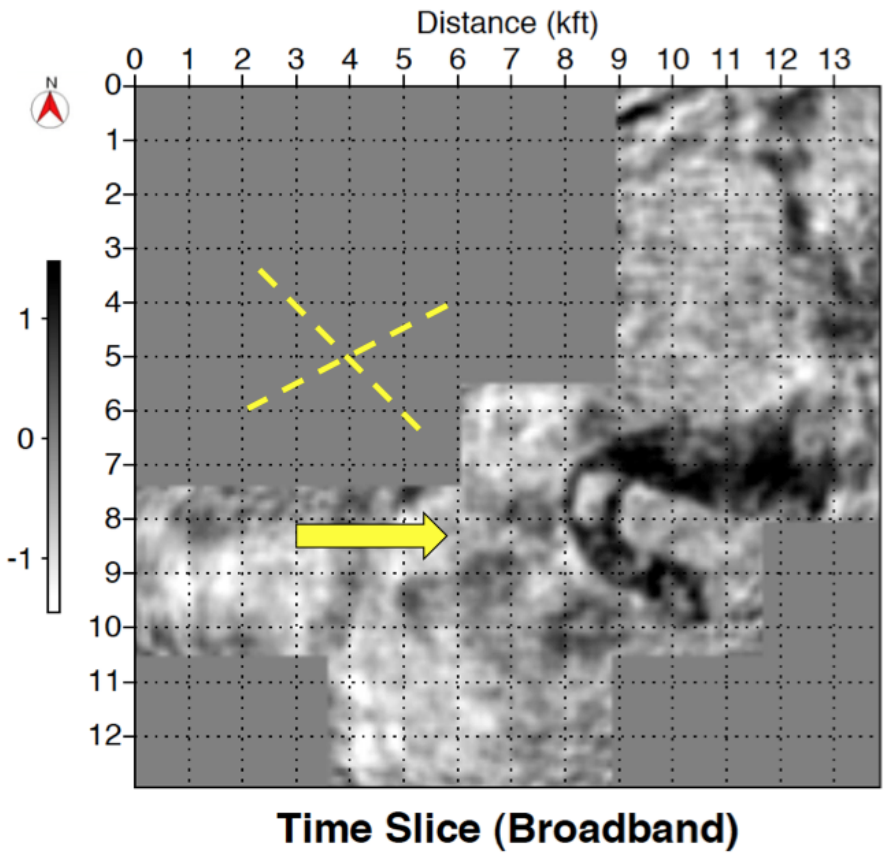

Figure 11. Broadband timeslice at 848 ms, approximately coincident with the Miss/Penn unconformity. Features observed in narrow band data (Figs 12 and 13) but not on the broadband data are indicated in yellow.

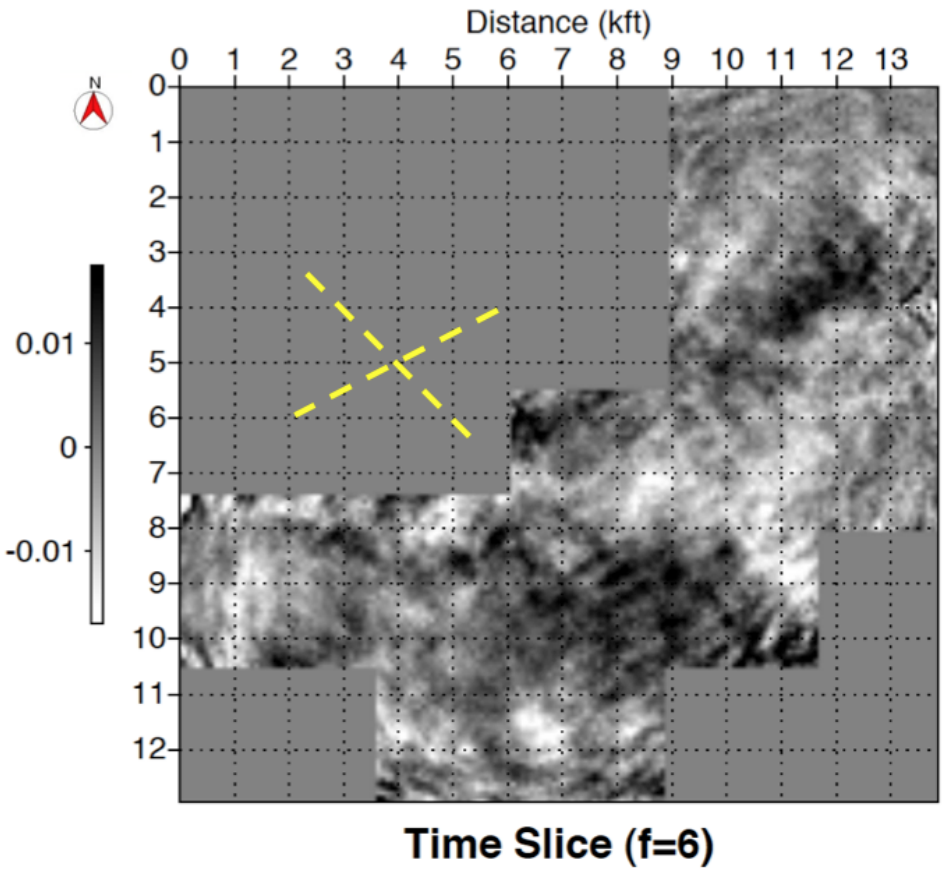

Figure 12. Narrow band (6 Hz) timeslice at 848 ms. Yellow dash lines indicate orientation of diagonal features (perhaps related to fractures) not seen in Fig 10.

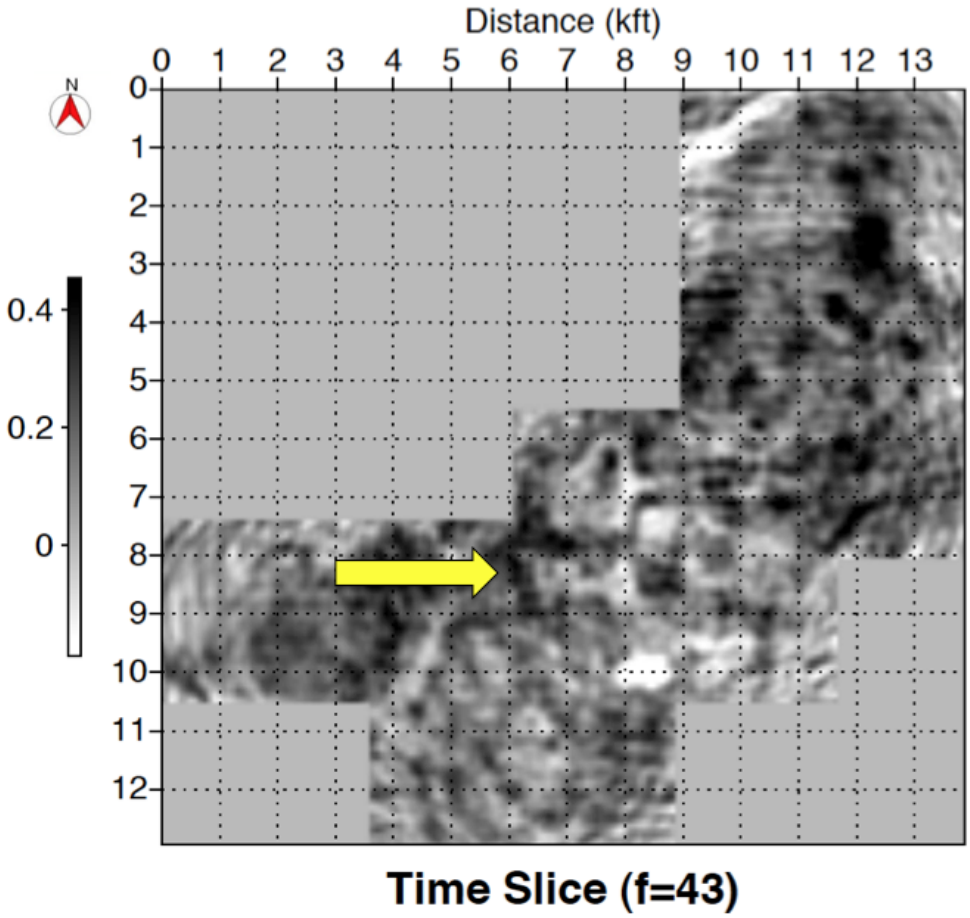

Figure 13. Narrow band (43 Hz) timeslice at 848 ms. Yellow arrow indicates channel feature not seen in Figure 10.

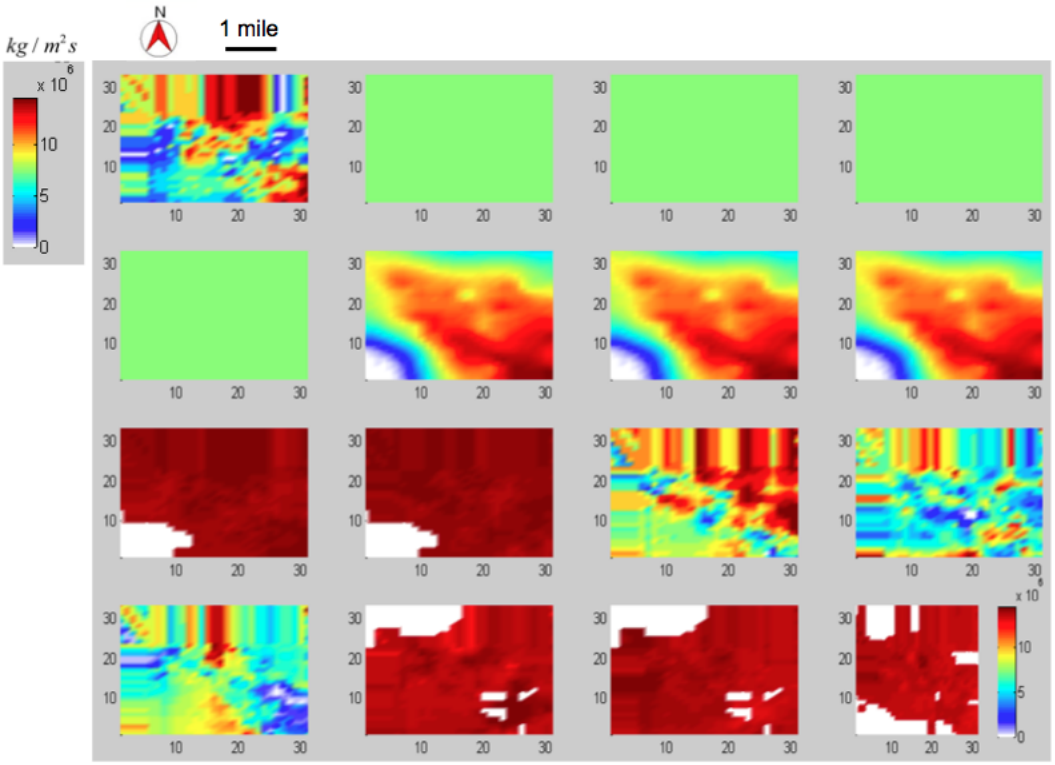

Figure 14: Impedance values calculated for the first 16 depth layers of the flow simulatino grid. Layer numbers progress across rows starting with 1 in the upper left. White space in certain layers indicate missing section due to an unconformity.

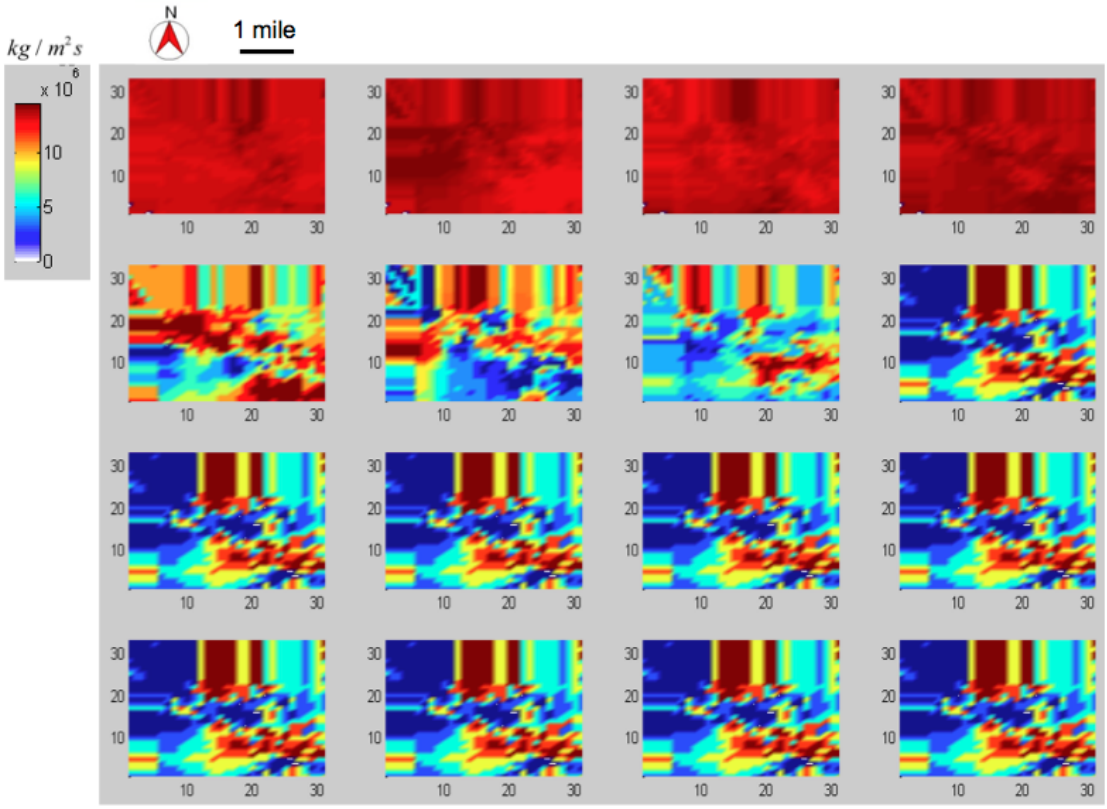

Figure 15: Impedance values for layers 17 to 32. Stripes in the simulation grid output parameters are likely sparse data interpolation artifacts that had little effect on flow simulation but will be important for seismic simulation.

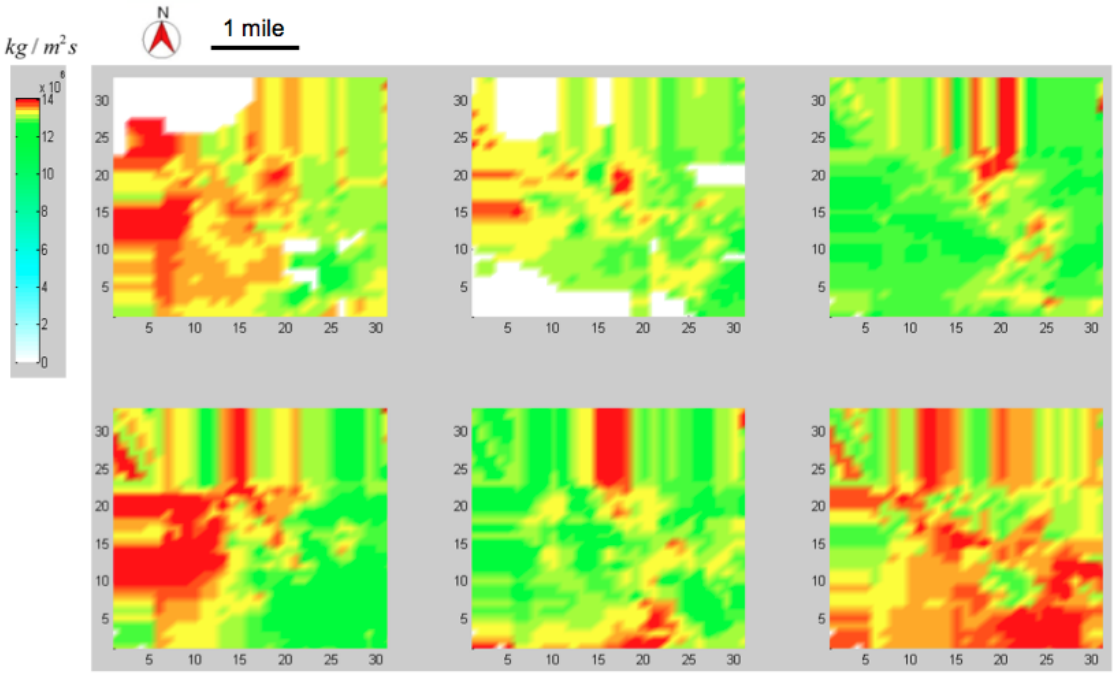

Figure 16. Impedance distribution from depth layers 15-20, which span the unconformity.

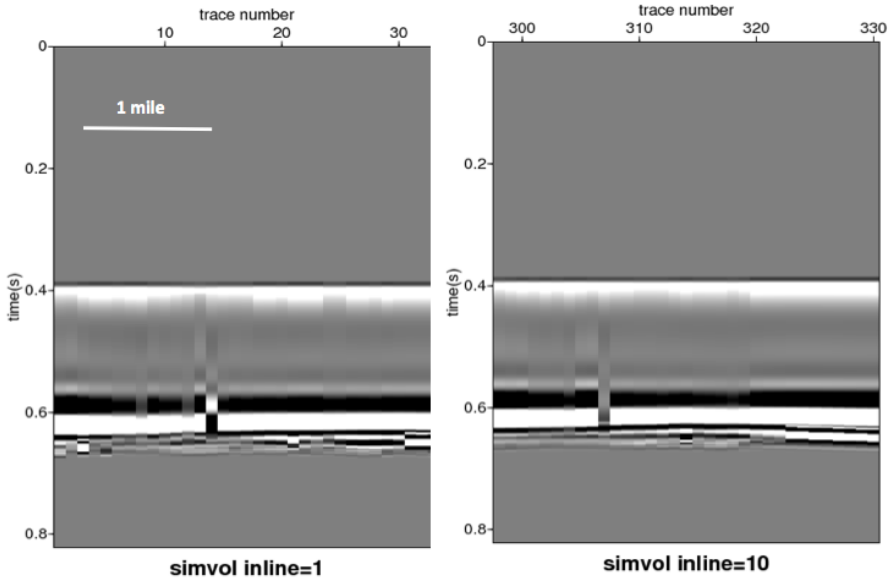

Figure 17a. Seismic data simulated from flow grid parameters and the Gassmann theory. This represents intital conditions before simulated CO2 injection. The first strong reflection appearing at 0.4 s the upper surface of the flow grid model. Reflections near 0.6 s are associated with an unconformity.

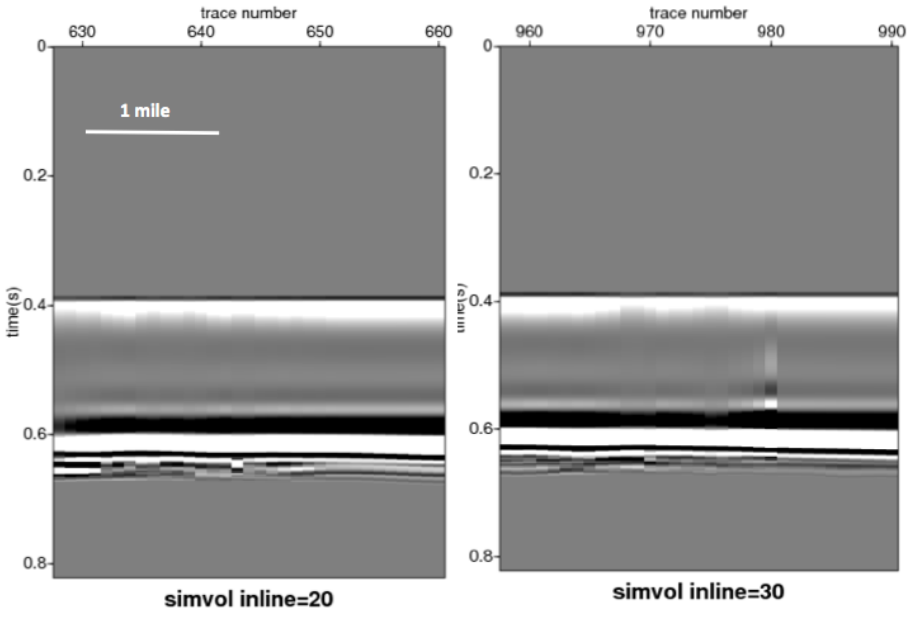

Figure 17b. Same as Fig 17a for two additional lines.

Sidebottom 6	Humphrey 4-18
• Density (errors)	• DT (errors)
• RHOB (errors)	• DT_CLIP
• RHOB_CLIP	• RHOB (errors)
• Sonic	• RHOB_CLIP

Figure 18. Logs Available for synthetics.

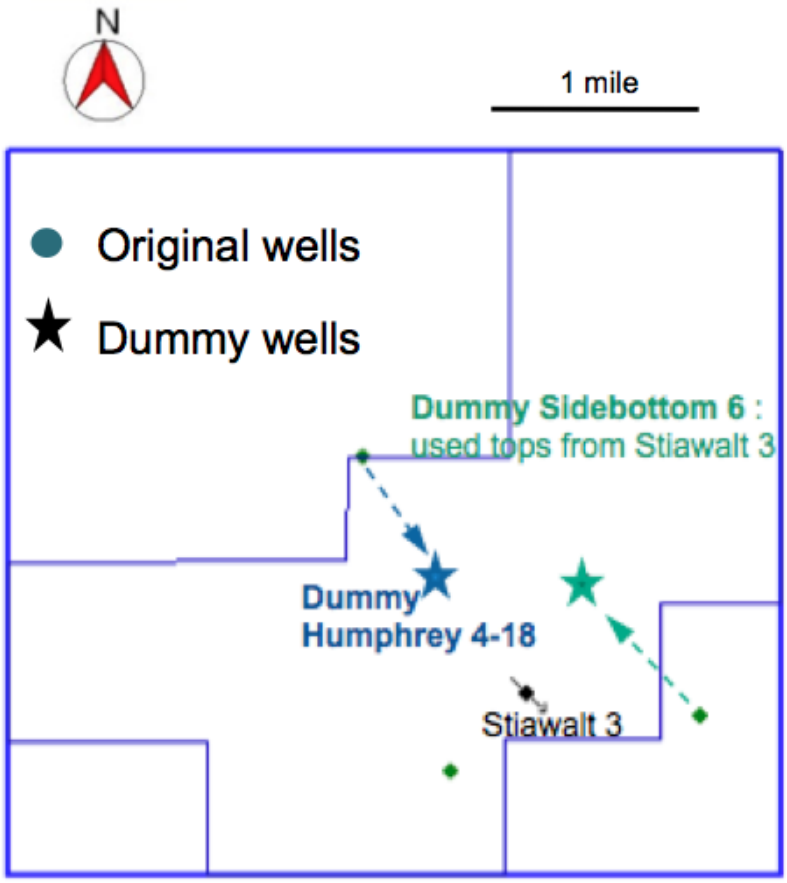

Figure 19. Dummy well locations

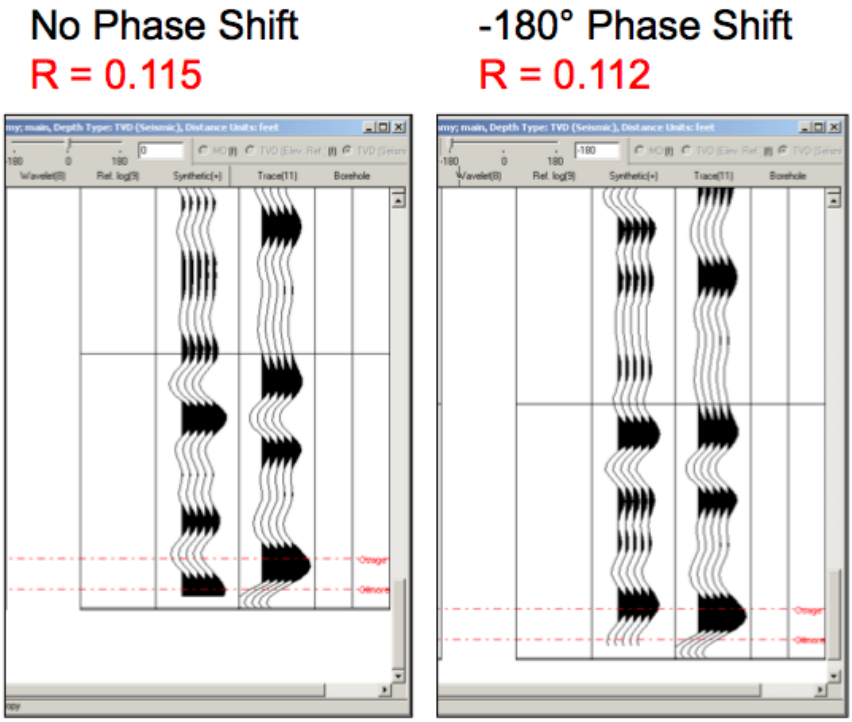

Figure 20. Dummy Humphrey 4-18 synthetic before and after phase shift. Constructed using clipped logs

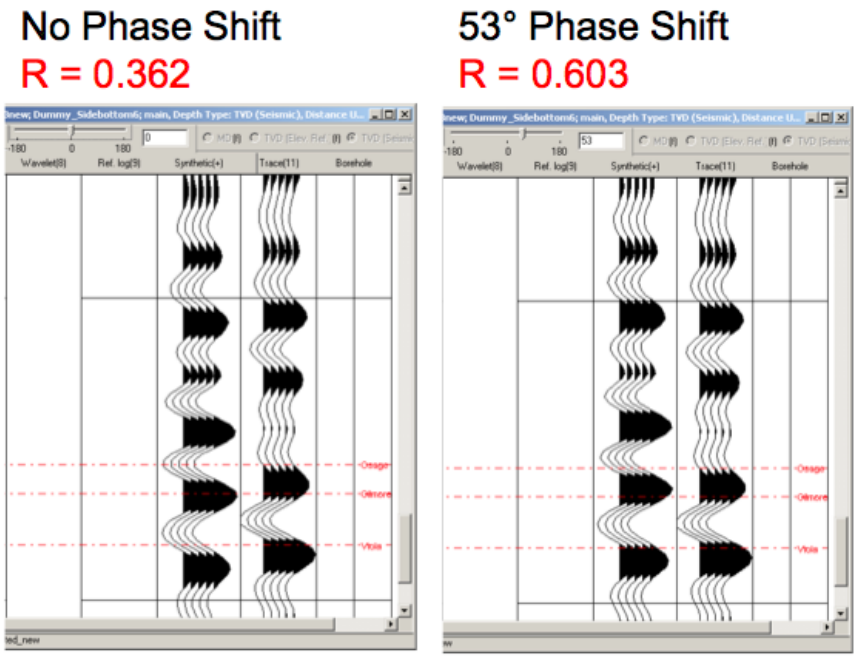

Figure 21. Dummy Sidebottom 6 synthetic wavelet before and after phase shift. Constructed using original sonic log and clipped density log.

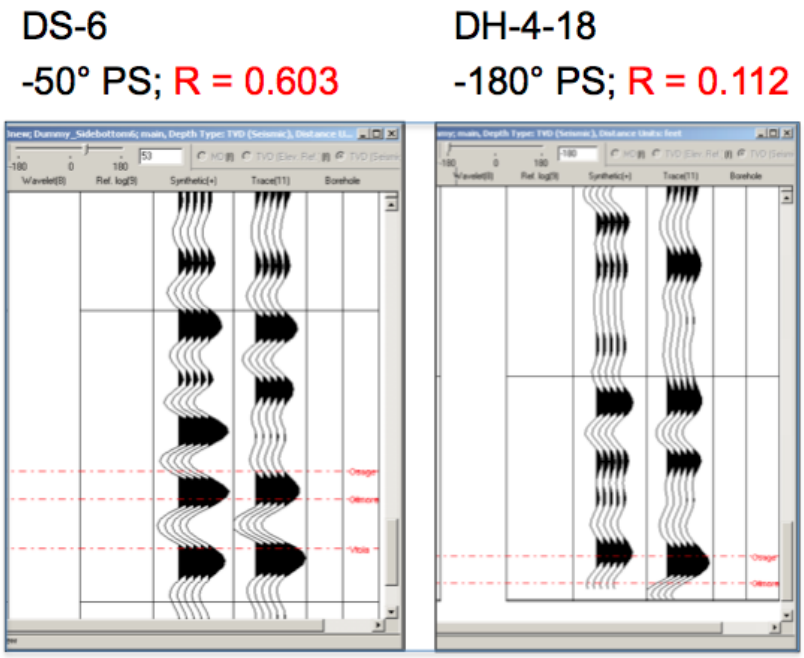

Figure 22. Comparison between synthetic seismograms from each well. Sidebottom 6 shows a better match and yields a much better R-value.

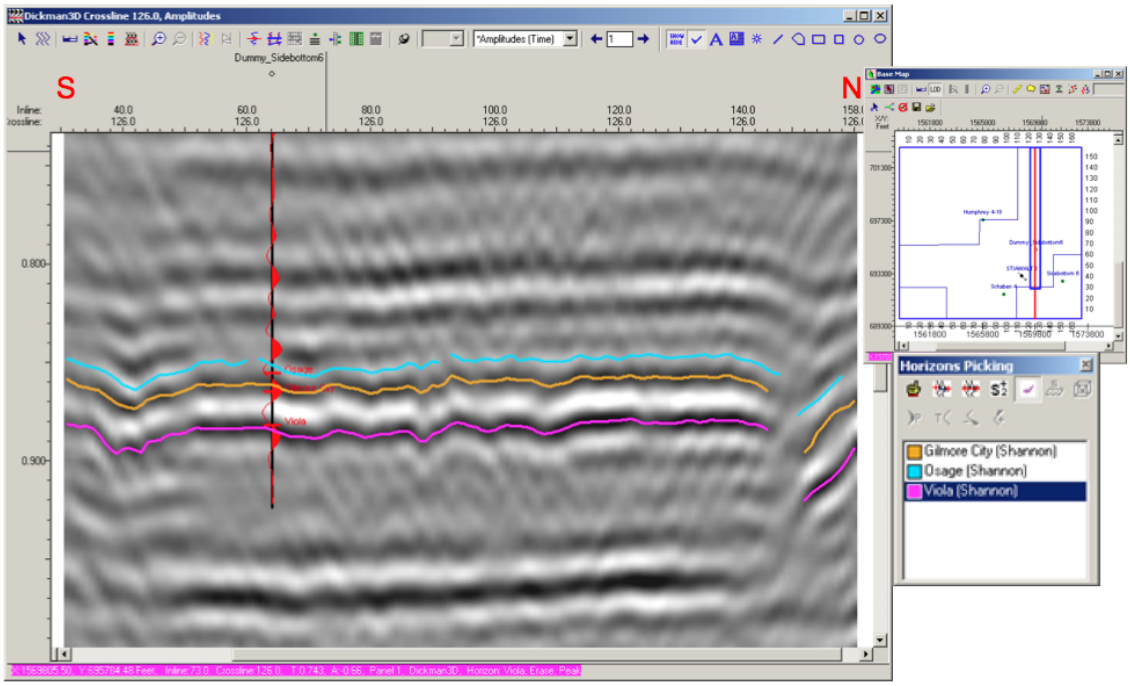

Figure 23. Dummy synthetic shown in vertical section Osage picked at trough, Gilmore City at peak, Viola at peak.